

Resonant Scattering and Microscopic Model of Spinless Fermi Gases in One-dimensional Optical Lattices

Xiaoling Cui

Beijing National Laboratory for Condensed Matter Physics,
Institute of Physics, Chinese Academy of Sciences, Beijing 100190, China
(Dated: July 26, 2021)

We study the effective Bloch-wave scattering of a spinless Fermi gas in one-dimensional (1D) optical lattices. By tuning the odd-wave scattering length, we find multiple resonances of Bloch-waves scattering at the bottom (and the top) of the lowest band, beyond which an attractive (and a repulsive) two-body bound state starts to emerge. These resonances exhibit comparable widths in the deep lattice limit, and the finite interaction range plays an essential role in determining their locations. Based on the exact two-body solutions, we construct an effective microscopic model for the low-energy scattering of fermions. The model can reproduce not only the scattering amplitudes of Bloch-waves at the lowest band bottom/top, but also the attractive/repulsive bound states within a reasonably large energy range below/above the band. These results lay the foundation for quantum simulating topological states in cold Fermi gases confined in 1D optical lattices.

Introduction. As a prominent example of quantum simulation, an odd-wave interacting Fermi gas in one-dimensional(1D) optical lattices can serve as an ideal platform for realizing the Kitaev chain model[1], a prototype of system hosting Majorana fermions[2] and recently attracting great attention in condensed matter physics[3]. Nevertheless, to achieve the goal of quantum simulation using cold atoms, it is fundamentally important to understand the two-body scattering property of a dilute gas as the first step. For instance, it has been found that the interplay between strong s-wave interaction and lattice potential can significantly modify the low-energy scattering property of Bloch waves[4–9]. Lattices can also support a peculiar type of repulsive bound state that is excluded in continuum[10]. Furthermore, the correct understanding of two-body scattering property is the foundation to construct an effective low-energy model, which will facilitate the study of many-body physics as the next step.

In this work, we exactly solve the two-body effective scattering of odd-wave interacting (spinless) fermions in 1D optical lattices. We adopt a two-channel Hamiltonian that naturally incorporates the effect of finite interaction range, as a realistic situation in cold atoms when reducing the 3D p-wave interacting Fermi gas[11–14] to quasi-1D by transverse confinement[15–18]. Based on the recently developed interaction renormalization approach for 1D odd-wave systems[19, 20], our formulism are able to capture all the high-band effects and applicable to arbitrary lattice depths and interaction strengths/ranges. The main findings include (i) the multiple Bloch-wave resonances by tuning odd-wave scattering strengths and associated attractive/repulsive bound states; (ii) the sensitive dependence of resonance locations and widths on the interaction range and the lattice depth; (iii) an effective model constructed for lowest-band fermions, which correctly predicts both the scattering amplitudes of Bloch waves and the bound states below/above the lowest band. These results reveal the unique scattering property due to

the interplay of odd-wave interactions and lattice potentials, and pave the way for future exploring the physics of Majorana fermions in cold atomic gases.

Formulism. We start from a two-channel Hamiltonian:

$$\mathcal{H} = \int dx (\psi^\dagger h_f \psi + d^\dagger h_d d + U_{fd}) ; \quad (1)$$

$$U_{fd} = \frac{g}{2} (d^\dagger [(i\partial\psi)\psi - \psi(i\partial\psi)] + h.c.) .$$

Here ψ^\dagger and d^\dagger are respectively the creation operators of open-channel fermions and closed-channel dimers under single-particle Hamiltonian $h_f = -\partial_x^2/(2m) + V_f(x)$ and $h_d = -\partial_x^2/(4m) + \nu + V_d(x)$, with lattice potentials $V_f = V_0 \sin^2(\pi x/a_L)$ and $V_d = 2V_f(x)$; ν is the closed-channel detuning, and g is the coupling strength between two channels. The free-space scattering length l_o and effective range r_o for odd-wave interaction are defined through renormalization equations[19, 20]:

$$\frac{m}{2l_o} = -\frac{\nu}{2g^2} + \frac{1}{L} \sum_q \frac{q^2}{2\epsilon_q} ; \quad (2)$$

$$r_o = \frac{1}{m^2 g^2} ; \quad (3)$$

where $\epsilon_q = q^2/(2m)$ and L is the length of the system. Here we consider the p-wave resonance of identical ^{40}K fermions near 200G[11, 12] under a tight transverse confinement with frequency ω_\perp , and ω_\perp sets the largest energy scale in this paper so that the system is effectively in 1D regime. Given $a_\perp = 1/\sqrt{m\omega_\perp} \sim 50\text{nm}$ and a large 3D p-wave range $\sim 4 \times 10^6 \text{cm}^{-1}$, an estimation based on Ref.[16–18] gives $r_o \sim 250\text{nm}$, which is about half of typical lattice spacing $a_L \sim 500\text{nm}$. Thus in this paper we take $r_o = 0.5a_L$ and use $k_L = \pi/a_L$ and $E_L = k_L^2/(2m)$ as the units of momentum and energy, respectively. In particular, we scale the lattice depth as $v \equiv V_0/E_L$.

Expanding ψ, ψ^\dagger and d, d^\dagger in terms of the Bloch wave eigenstates of h_f and h_d , the Hamiltonian (1) can be

rewritten as:

$$\mathcal{H} = \sum_{nk} \epsilon_{nk} \psi_{nk}^\dagger \psi_{nk} + \sum_{NK} (E_{NK} + \nu) d_{NK}^\dagger d_{NK} + \frac{g}{\sqrt{L}} \sum_{NK} \sum_{nn';kk'} \left(c_{nn';kk'}^{NK} d_{NK}^\dagger \psi_{nk} \psi_{n'k'} + h.c. \right) \quad (4)$$

Here ϵ_{nk} and E_{NK} are respectively the Bloch-wave energies of fermions and dimers, with $n, N = \{0, 1, 2, \dots\}$ the band index and $k, K \in (-k_L, k_L]$ the crystal momentum, and $c_{nn';kk'}^{NK}$ is the atom-dimer coupling constant. One can check that a non-zero $c_{nn';kk'}^{NK}$ requires $k + k'$ identical to K up to an integer number of $2k_L$. Therefore K is a good number during the scattering process.

We write down the two-body ansatz with given K :

$$|\Psi\rangle_K = \frac{1}{2} \sum_{nn'} \sum_k \alpha_{nn';k}^K \psi_{nk}^\dagger \psi_{n',[K-k]}^\dagger + \sum_N \beta_N^K d_{NK}^\dagger, \quad (5)$$

here $[.]$ is to shift $K - k$ by an integer number of $2k_L$ to be within $(-k_L, k_L]$. By imposing the Schrödinger equation $\mathcal{H}|\Psi\rangle_K = E|\Psi\rangle_K$, we obtain the coupled equations:

$$(E - \epsilon_{nk} - \epsilon_{n',[K-k]}) \alpha_{nn';k}^K = 2g \sum_N c_{nn';k,[K-k]}^{NK*} \beta_N^K; \quad (6)$$

$$(E - E_{NK} - \nu) \beta_N^K = g \sum_{nn';k} c_{nn';k,[K-k]}^{NK} \alpha_{nn';k}^K \quad (7)$$

By eliminating $\alpha_{nn';k}^K$, these equations can be reduced to

$$\left(\frac{m}{2l_o} - M_{NN}^K \right) \beta_N^K = \sum_{N' \neq N} M_{NN'}^K \beta_{N'}^K \quad (8)$$

with

$$M_{NN'}^K = \left(-\frac{m^2 r_o}{2} (E - E_{NK}) + \frac{1}{L} \sum_k \frac{k^2}{2\epsilon_k} \right) \delta_{NN'} + \frac{1}{L} \sum_{nn';kk'} \frac{c_{nn';kk'}^{NK} c_{nn';kk'}^{N'K*}}{E - \epsilon_{nk} - \epsilon_{n'k'}}. \quad (9)$$

Note that the relation $k' = [K - k]$ is hidden in above summation to ensure the finite $c_{nn';kk'}^{NK}$. In writing Eqs.(8,9), we have also utilized the renormalization equations (2,3)[19, 20]. We see that here the lattice affects the low-energy solution (E) through the modification of spectra (ϵ_{nk} , E_{NK}) and couplings ($c_{nn';kk'}^{NK}$). Since the lattice does not affect the scattering in high-energy space, the two ultraviolet divergences in M_{NN}^K can exactly cancel with each other.

We remark that Eq.8 can apply to different interaction strengths/ranges, lattice depths and total momenta for spinless fermions scattering in 1D lattices. Its left and right sides respectively describe the scattering process within each dimer level and between different levels, while the latter is caused by the coupling between relative and center-of-mass motions due to the presence of

lattice potentials[21]. Here we will focus on the two-body ground state with $K = 0$, and simplify $c_{nn';kk'}^{N,K=0}$ as $c_{nn';k}^N$.

Bound state spectrum. The bound state solution $E = E_b$ can be obtained by requiring nontrivial solutions of $\{\beta_N^K\}$ in Eq.8. In Fig.1a, we show E_b as a function of $1/l_o$ at given $r_o = 0.5a_L$ and $v = 6$. As increasing $1/l_o$, we can see a series of bound states emerging from the two-body continuum, corresponding to the coupled-channel ($\{N\}$) solutions in Eq.8. Given the property that $M_{NN'}$ is finite only for even $N - N'$, these bound states fall into two classes: one is by coupling dimer levels with even N (solid lines in Fig.1a), which produces an even-parity two-body wave-function in the center-of-mass motion: $\Psi(x_1, x_2) = \Psi(-x_2, -x_1)$; the other is by coupling all odd- N levels (dashed lines) and produces an odd-parity wave function: $\Psi(x_1, x_2) = -\Psi(-x_2, -x_1)$. We see that the ground state belongs to the even-parity class.

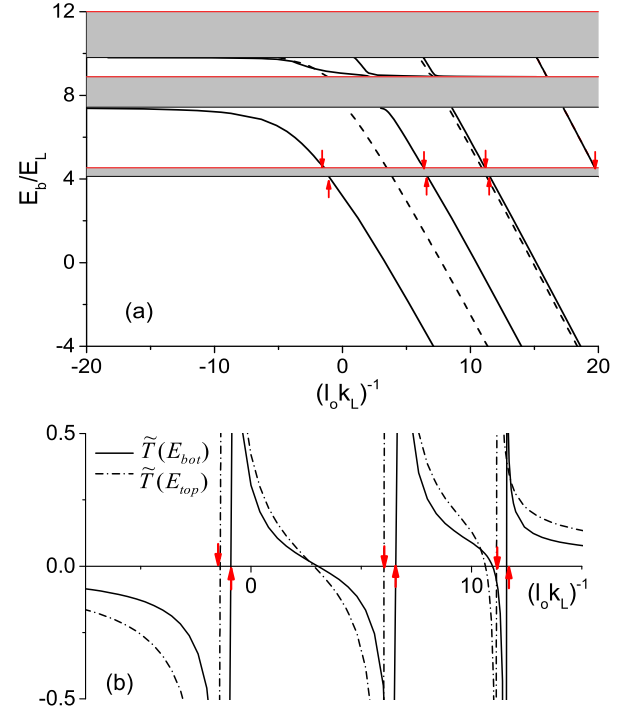


FIG. 1. (Color online). (a) Bound state energy E_b (in unit of E_L) and (b) the scaled T-matrix \tilde{T} (in unit of $(mLk_L)^{-1}$) for Bloch-wave scattering near the lowest band bottom (solid lines) and top (dashed-dot) as functions of $(l_o k_L)^{-1}$. Here $v = 6$, $r_o = 0.5a_L$. In (a), the solid (dashed) lines correspond to even-parity (odd-parity) center-of-mass motions (see text). The upward (downward) arrows in (a,b) mark the emergence of attractive (repulsive) bound states near the lowest band, where $\tilde{T}(E_{bot})$ ($\tilde{T}(E_{top})$) go across resonances.

Bloch-wave resonance. The bound states emergent at the bottom and top of each continuum band in Fig.1a imply the scattering resonances of Bloch waves at corresponding energy. In general, for any two-body scattering state $\Psi(E) = |n, k_0; n', -k_0\rangle$ (E is the total energy), the

on-shell scattering matrix $T(E)$ can be obtained by summing up all virtual scatterings involving the dimer and two-fermion intermediate states[20]. The resulting $T(E)$ can be expressed[7] by introducing the eigenvectors R_N^α and eigenvalues χ_α for M-matrix (Eq.9), which gives

$$T(E) = 2 \sum_{\alpha} \frac{|\sum_N R_N^\alpha c_{nn'k_0}^N|^2}{\frac{m}{2l_o} - \chi_\alpha}. \quad (10)$$

Once $m/(2l_o)$ matches one of the eigenvalues χ_α , $T(E)$ will go through a resonance, with the width determined by the nominator of above equation.

In Fig.1b, we plot the scaled T-matrix, $\tilde{T} = T/\Delta k^2$, for Bloch states scattering near the lowest-band bottom ($\Delta k = k_0 \rightarrow 0$) and the top ($\Delta k = k_L - k_0 \rightarrow 0$) at $v = 6$, respectively denoted by $\tilde{T}(E_{bot})$ and $\tilde{T}(E_{top})$. Multiple resonances are shown as tuning $1/l_o$. As only the even-N dimer levels couple with the lowest-band scattering state, these resonances are associated with the labels $\alpha = 0, 2, 4, \dots$ in Eq.(10). Combined with Fig.1a, one can see that the emergences of attractive (or repulsive) bound states correspond to the resonance of $\tilde{T}(E_{bot})$ from $-\infty$ to $+\infty$ (or $\tilde{T}(E_{top})$ from $+\infty$ to $-\infty$).

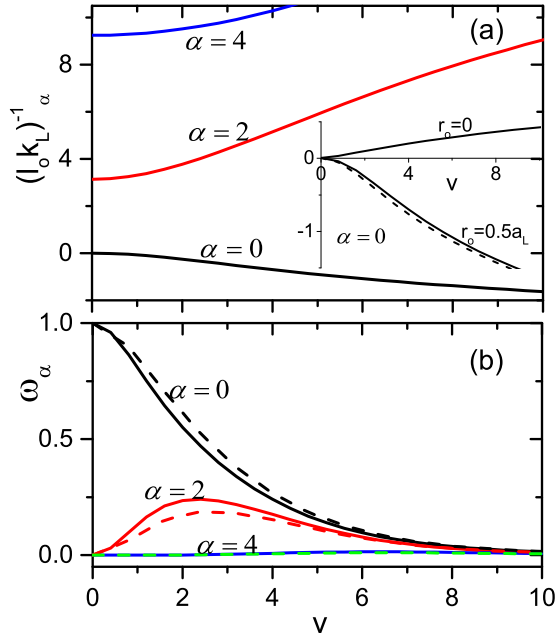


FIG. 2. (Color online). Resonance locations $(l_o k_L)_\alpha^{-1}$ (a) and widths ω_α (b) as functions of v for the first three resonances of $\tilde{T}(E_{bot})$ in Fig.1b. Inset of (a) shows $(l_o k_L)_{\alpha=0}^{-1}$ with zero and finite ranges; the dashed line shows the prediction to finite-range case based on the decoupled-channel analysis (see text). Dashed lines in (b) shows $(c_{00;k_0}^{N=\alpha}/k_0)^2$ as $k_0 \rightarrow 0$.

In Fig.2(a,b), we plot the resonance locations $(l_o k_L)_\alpha^{-1}$ and widths $\omega_\alpha = |\sum_N R_N^\alpha c_{00k_0}^N|^2/k_0^2$ for the first three resonances of $\tilde{T}(E_{bot})$ as a function of v . We can see that as v increases from zero, the first resonance ($\alpha = 0$)

moves from $1/l_o = 0$ (free-space resonance) to $1/l_o < 0$ side (weak coupling), with decreasing resonance width; while the rest ones ($\alpha = 2, 4$) move to $1/l_o > 0$ side (strong coupling), with the widths initially increasing and then decreasing. As shown below, these results uniquely manifest the interplay between lattices and odd-wave interactions with finite range.

First, we analyze the finite range effect to the resonance locations. For comparison, in the inset of Fig.2a we plot the first resonance locations ($\alpha = 0$) for both finite and zero r_o . Contrary to the finite r_o case, with zero r_o the resonance moves to $1/l_o > 0$ side as increasing v . A qualitative understanding can be gained from the decoupled-channel assumption, i.e., by neglecting all $M_{N \neq N'}$ in Eq.9. In this case the resonance is solely determined by matching M_{NN} with $m/2(1/l_o + \Delta_N)$, with $\Delta_N = m r_o (E_{bot} - E_{N0})$ denoting the difference of the N-th resonance locations between zero and finite r_o cases. As shown in the inset of Fig.2a, $\Delta_{N=0} (> 0)$ can well approximate the real difference for the first resonance. In large v limit, $(E_{bot} - E_{00})$ is roughly the zero-point energy for the relative motion of two atoms in a single well, so we expect the first resonance occur in the very weak coupling regime $1/l_o \sim -v^{1/2} r_o / a_L^2$. Note that this should be distinguished from the induced resonance in 3D lattices with arbitrarily weak s-wave interaction[4, 6, 7], where the enhanced on-site coupling, rather than the range effect, plays a dominated role.

Second, the behavior of ω_α can also be qualitatively understood from the decoupled-channel analysis, where $R_N^\alpha = \delta_{N\alpha}$ and $\omega_\alpha = (c_{00k_0}^\alpha/k_0)^2$, as shown by dashed lines in Fig.2b. A remarkable feature here is that all ω_α decay with v in large v limit. Physically, this is because the odd-wave interaction uniquely favors fermion-fermion correlation between neighboring lattice sites, which can be greatly suppressed by the potential barrier of deep lattices. This is in sharp contrast to the s-wave interaction case, where one of resonance widths can be greatly enhanced by on-site correlations for deep lattices[7]. Here due to the comparable widths for large v (see Fig.2b, $\omega_{0,2}$ are of the same order for $v \geq 4$), one has to treat multiple Bloch-wave resonances at equal footing.

Effective model. Based on the two-body solutions, we can construct an effective model, H_{eff} , for open-channel fermions in the lowest band. Namely, H_{eff} corresponds to projecting the original fermion operators in Eqs.(1,4) to the lowest band, while for the dimer part we keep all the bands involved considering the multiple resonances that should be treated equally in general. Accordingly, the detuning ν and coupling g are then replaced by the effective ones ν_{eff} and g_{eff} . These two parameters resulted in an effective interaction strength U_{eff} and a finite range r_{eff} :

$$U_{eff} = -2 \frac{g_{eff}^2}{\nu_{eff}}; \quad r_{eff} = -\frac{1}{m^2 g_{eff}^2}. \quad (11)$$

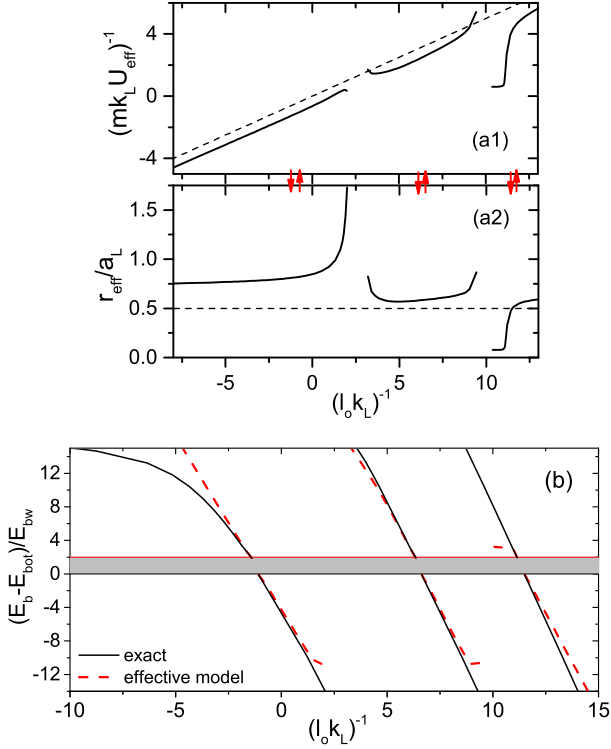


FIG. 3. (Color online). (a1,a2) Effective parameters U_{eff}^{-1} and r_{eff} near the resonances in Fig.1b. The dashed lines show the free space results: $U_{\text{eff}} = 2l_o/m$ and $r_{\text{eff}} = r_o = 0.5a_L$. The up- and down-ward arrows mark the resonance positions of $\tilde{T}(E_{\text{bot}})$ and $\tilde{T}(E_{\text{top}})$. (b) Bound state spectrum from exact solutions (black solid, same as Fig.1a) and from effective model (red dashed) near the lowest band. Here energies are scaled by the single-particle band width E_{bw} .

As U_{eff} and r_{eff} have encapsulated all contributions from higher-band scatterings, they can be seen as *regularized* interaction parameters for the lowest-band fermions.

We determine U_{eff} and r_{eff} by matching the T-matrix from effective model (T_{eff}) with the exact values (T in Eq.10) for Bloch-wave scattering at the bottom and the top of the lowest band. Specifically, T_{eff} reads

$$T_{\text{eff}}(E) = 2 \sum_{\alpha} \frac{|\sum_N \bar{R}_N^{\alpha} c_{00;k}^{N}|^2}{\frac{1}{U_{\text{eff}}} - \bar{\chi}_{\alpha}}, \quad (12)$$

where \bar{R}_N^{α} and $\bar{\chi}_{\alpha}$ are respectively the eigenvector and eigen-value of the matrix $\bar{M}(E)$ with elements:

$$\bar{M}_{NN'} = -\frac{m^2 r_{\text{eff}}}{2} (E - E_{NK}) \delta_{NN'} + \frac{1}{L} \sum_k \frac{c_{00k}^{N*} c_{00k}^{N'}}{E - \epsilon_{0k} - \epsilon_{0,-k}},$$

Thus Eq.12 can also predict multiple scattering resonances. Since both T and T_{eff} are multi-value functions of interaction parameters, to ensure a one-to-one mapping between $1/l_o$ and $1/U_{\text{eff}}$, we require T and T_{eff} are near the same order of resonance (α), i.e., dominated

by the same dimer level. Such procedure leads to the solution of U_{eff} and r_{eff} as shown in Fig.3(a1,a2), which reproduce both $\tilde{T}(E_{\text{bot}})$ and $\tilde{T}(E_{\text{top}})$ in Fig.1b. We can see that both U_{eff} and r_{eff} differ from the free-space results $2l_o/m$ [19] and $0.5a_L$ (dashed lines), due to the renormalized high-band contributions. We have not determined U_{eff} and r_{eff} far from resonances, as in this regime the resonance order (α) is obscure to identify.

We test the validity of H_{eff} by calculating the bound state energy E_b , which is determined by the divergence of T_{eff} in Eq.12 at $E = E_b$. As shown in Fig.3b, E_b can well reproduce the exact solutions for attractive and repulsive bound states near Bloch-wave resonances, even within an energy range up to 5 – 10 times the single-particle band width for the first two resonances. Meanwhile, we note that the effective model only works in a very narrow window for the bound states near the third resonance. This can be attributed to its extremely narrow width $\omega_4 \sim 0.014 \ll \omega_{0,2}$ (see Fig.2b). Accordingly, outside the resonance regime the associated bound states have much less weight in the lowest band, and the effective model desired for lowest-band fermions fails to work there.

To this end, we have confirmed the validity of H_{eff} in predicting both the scattering amplitudes and the bound states above/below the lowest-band near the Bloch-wave resonances. Our scheme here to determine the effective parameters in H_{eff} is distinct from previous studies on s-wave interacting fermions [8, 9, 22]. We have also checked that the single-channel model, i.e., without including closed-channel dimers [7], is unable to predict the correct bound states in this case.

Finally, we convert H_{eff} to lattice model by expanding field operators in terms of Wannier functions, $\psi(x) = \sum_i \psi_i \omega_0(x - R_i)$; $d(x) = \sum_{N,i} d_{N,i} W_N(x - R_i)$, giving

$$H_{\text{eff}} = -t_f \sum_{\langle i,j \rangle} (\psi_i^{\dagger} \psi_j + h.c.) - \sum_{\langle i,j \rangle; N} t_d^{(N)} (d_{N,i}^{\dagger} d_{N,j} + h.c.) + \sum_i \epsilon_f \psi_i^{\dagger} \psi_i + \sum_i (\epsilon_d^{(N)} + \nu_{\text{eff}}) d_{N,i}^{\dagger} d_{N,i} + g_{\text{eff}} \sum_{N,i,\delta_1,\delta_2} (c_{\delta_1,\delta_2}^{(N)} d_{N,i+\delta_1}^{\dagger} \psi_i \psi_{i+\delta_2} + h.c.), \quad (13)$$

where t_f and ϵ_f ($t_d^{(N)}$ and $\epsilon_d^{(N)}$) are the nearest-neighbor hopping and on-site potential of fermions (dimers at level N); the coupling $c_{\delta_1,\delta_2}^{(N)} = -i \int dx W_N^*(x - \delta_1 a_L) (\omega_0'(x) \omega_0(x - \delta_2 a_L) - \omega_0(x) \omega_0'(x - \delta_2 a_L))$. Fixing $\delta_2 = 1$, we show in Fig.4a that $|c_{\delta_1,\delta_2}^{(N)}|$ is the largest when $\delta_1 = 0$ or 1. We have checked that for a general δ_2 , $|c_{\delta_1,\delta_2}^{(N)}|$ is the largest when $\delta_1 = [\delta_2/2]$ or $[(\delta_2 + 1)/2]$, i.e., when the dimer sits in the center of two fermions to optimize the atom-dimer coupling. In Fig.4b, we plot the largest $|c_{\delta_1,\delta_2}^{(N)}|$ as a function of δ_2 , and find it gradually decreases as δ_2 increases from 1. Thus to capture the most dominated atom-dimer coupling in deep lattices, we can choose the nearest-neighbor fermions ($\delta_2 = 1$) and the

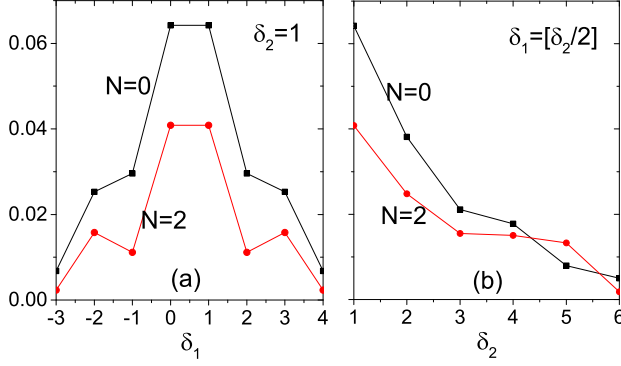


FIG. 4. (Color online). Lattice parameter $|c_{\delta_1, \delta_2}^{(N)}|$ (in unit of $a_L^{-3/2}$) for $N = 0, 2$ at $v = 6$. In (a) $\delta_2 = 1$; in (b) $\delta_1 = [\delta_2/2]$.

dimers sitting with either one of them ($\delta_1 = 0, 1$).

Compare the lattice Hamiltonian (Eq.13) with the Kitaev chain model[1], one can expect that if the dimers condense, they will play the role of pairing mean-field in the Kitaev model and thus reproduce the Majorana physics. Meanwhile, the existence of quantum fluctuations, the resonant scatterings, and the multi-level structure of dimers in the current system are all beyond the Kitaev model. Their interplay will promisingly result in a richer many-body property in such atomic system, which is to be explored in future.

Summary. In summary, we have addressed the two-body effective scattering and bound states for 1D Fermi gases in optical lattices across odd-wave resonances. The multiple Bloch-wave resonances with comparable widths, the associated attractive/repulsive bound states, and the effect of finite interaction range can be detected in current cold atoms experiments. In addition, we have constructed an effective low-energy model, which successfully describes both the scattering amplitudes and bound states near the lowest band. As an analog of the Kitaev chain to host Majorana fermions[1], the effective model sets the basis for future exploring topological quantum states in realistic 1D cold atomic systems.

Acknowledgment. The work is supported by the National Natural Science Foundation of China (No.11626436, No.11374177, No. 11421092, No. 11534014), the National Key Research and Development

Program of China (2016YFA0300603), and the National Science Foundation under Grant No. NSF PHY11-25915. The author would like to thank the hospitality and support of the Kavli Institute for Theoretical Physics in Santa Barbara during the program "Universality in Few-Body Systems" in the winter of 2016, where this manuscript was partly finished.

-
- [1] A.Y. Kitaev, Phys. Usp. **44**, 131 (2001).
 - [2] E. Majorana, Nuovo Cimento **5**, 171 (1937).
 - [3] F. Wilczek, Nat. Phys. **5**, 614 (2009); S. R. Elliott and M. Franz, Rev. Mod. Phys. **87**, 137 (2015).
 - [4] P. O. Fedichev, M. J. Bijlsma, and P. Zoller, Phys. Rev. Lett. **92**, 080401 (2004).
 - [5] R. B. Diener and T.-L. Ho, Phys. Rev. Lett. **96**, 010402 (2006).
 - [6] X. Cui, Y. Wang and F. Zhou, Phys. Rev. Lett. **104**, 153201 (2010).
 - [7] H. P. Buchler, Phys. Rev. Lett. **104**, 090402 (2010).
 - [8] J. von Stecher, V. Gurarie, L. Radzihovsky, and A. M. Rey, Phys. Rev. Lett. **106**, 235301 (2011).
 - [9] M. L. Wall and L. D. Carr, Phys. Rev. Lett. **109**, 055302 (2012).
 - [10] K. Winkler, G. Thalhammer, F. Lang, R. Grimm, J. H. Denschlag, A. J. Daley, A. Kantian, H. P. Buechler and P. Zoller, Nature **441**, 853 (2006).
 - [11] C. A. Regal, C. Ticknor, J. L. Bohn, and D. S. Jin, Phys. Rev. Lett. **90**, 053201 (2003).
 - [12] C. Ticknor, C. A. Regal, D. S. Jin, and J. L. Bohn, Phys. Rev. A **69**, 042712 (2004).
 - [13] J. Zhang, E. G. M. van Kempen, T. Bourdel, L. Khaykovich, J. Cubizolles, F. Chevy, M. Teichmann, L. Tarruell, S. J. J. M. F. Kokkelmans, and C. Salomon, Phys. Rev. A **70**, 030702 (R)(2004).
 - [14] C. H. Schunck, M. W. Zwierlein, C. A. Stan, S. M. F. Raupach, W. Ketterle, A. Simoni, E. Tiesinga, C. J. Williams, and P. S. Julienne, Phys. Rev. A **71**, 045601 (2005).
 - [15] K. Gunter, T. Stoferle, H. Moritz, M. Kohl, and T. Esslinger, Phys. Rev. Lett. **95**, 230401 (2005).
 - [16] B. E. Granger and D. Blume, Phys. Rev. Lett. **92**, 133202 (2004).
 - [17] L. Pricoupenko, Phys. Rev. Lett. **100**, 170404 (2008).
 - [18] S.-G. Peng, S. Tan, and K. Jiang, Phys. Rev. Lett. **112**, 250401 (2014).
 - [19] X. Cui, Phys. Rev. A **94**, 043636 (2016).
 - [20] X. Cui and H. Dong, Phys. Rev. A **94**, 063650 (2016).
 - [21] Similar coupled equations also exist for s-wave interacting fermions in lattices, see Refs.[7, 9].
 - [22] L. M. Duan, Phys. Rev. Lett. **95**, 243202 (2005).

Resonant Scattering and Microscopic Model of Spinless Fermi Gases in One-dimensional Optical Lattices

Xiaoling Cui

Beijing National Laboratory for Condensed Matter Physics,
Institute of Physics, Chinese Academy of Sciences, Beijing 100190, China
(Dated: July 26, 2021)

We study the effective Bloch-wave scattering of a spinless Fermi gas in one-dimensional (1D) optical lattices. By tuning the odd-wave scattering length, we find multiple resonances of Bloch-waves scattering at the bottom (or the top) of the lowest band, beyond which an attractive (or a repulsive) two-body bound state starts to emerge. These resonances exhibit comparable widths in the deep lattice limit, and the finite interaction range plays an essential role in determining their locations. Based on the exact two-body solutions, we construct an effective microscopic model for the low-energy scattering of fermions. The model can reproduce not only the scattering amplitudes of Bloch-waves at the lowest band bottom/top, but also the attractive/repulsive bound states within a reasonably large energy range below/above the band. These results lay the foundation for quantum simulating topological states in cold Fermi gases confined in 1D optical lattices.

Introduction. As a prominent example of quantum simulation, an odd-wave interacting Fermi gas in one-dimensional(1D) optical lattices can serve as an ideal platform for realizing the Kitaev chain model[1], a prototype of system hosting Majorana fermions[2] and recently attracting great attention in condensed matter physics[3]. Nevertheless, to achieve the goal of quantum simulation using cold atoms, it is fundamentally important to understand the two-body scattering property of a dilute gas as the first step. For instance, it has been found that the interplay between strong s-wave interaction and lattice potential can significantly modify the low-energy scattering property of Bloch waves[4–9]. Lattices can also support a peculiar type of repulsive bound state that is exclusive in continuum[10]. Furthermore, the correct understanding of two-body scattering property is the foundation to construct an effective low-energy model, which will facilitate the study of many-body physics as the next step.

In this work, we exactly solve the two-body effective scattering of odd-wave interacting (spinless) fermions in 1D optical lattices. We adopt a two-channel Hamiltonian that naturally incorporates the effect of finite interaction range, as a realistic situation in cold atoms when reducing the 3D p-wave interacting Fermi gas[11–14] to quasi-1D by transverse confinement[15–18]. Based on the recently developed interaction renormalization approach for 1D odd-wave systems[19, 20], our formulism are able to capture all the high-band effects and applicable to any lattice depth and any interaction strength/range. The main findings include (i) the multiple Bloch-wave resonances by tuning odd-wave scattering strengths and associated attractive/repulsive bound states; (ii) the sensitive dependence of resonance locations and widths on the interaction range and the lattice depth; (iii) an effective model constructed for lowest-band fermions, which correctly predicts both the scattering amplitudes of Bloch waves and the bound states below/above the lowest band. These results reveal the unique scattering property due to

the interplay of odd-wave interactions and lattice potentials, and pave the way for future exploring the physics of Majorana fermions in cold atomic gases.

Formulism. We start from a two-channel Hamiltonian:

$$\mathcal{H} = \int dx \left\{ \psi^\dagger \left(-\frac{\partial_x^2}{2m} + V_f \right) \psi + d^\dagger \left(-\frac{\partial_x^2}{4m} + \nu + V_d \right) d + \frac{g}{2} (d^\dagger [(i\partial\psi)\psi - \psi(i\partial\psi)] + h.c.) \right\}. \quad (1)$$

Here ψ, ψ^\dagger and d, d^\dagger are the field operators of open-channel fermions and closed-channel dimers, respectively, subject to lattice potentials $V_f(x) = V_0 \sin^2(\pi x/a_L)$ and $V_d(x) = 2V_f(x)$; g is the odd-wave coupling strength between open- and closed-channel, and ν is the closed-channel detuning. The odd-wave scattering length l_o and the effective range r_o can be related to g and ν through renormalization equations[19, 20]: $m/(2l_o) = -\nu/(2g^2) + L^{-1} \sum_q q^2/(2\epsilon_q)$ and $r_o = (m^2 g^2)^{-1}$ (here $\epsilon_q = q^2/(2m)$; L is the length of the system). We consider the p-wave resonance of identical ^{40}K fermions near 200G[11, 12]. Given a large p-wave interaction range $\sim 4 \times 10^6 \text{cm}^{-1}$, and a tight transverse confinement with typical length $\sim 50 \text{nm}$, a rough estimation based on Ref.[16–18] result in $r_o \sim 250 \text{nm}$, which is about half of typical lattice spacing $a_L \sim 500 \text{nm}$. Thus in the main part of this paper, we will take $r_o = 0.5a_L$, and use $k_L = \pi/a_L$ and $E_L = k_L^2/(2m)$ as the units of momentum and energy, respectively. In particular, we scale the lattice depth as $v \equiv V_0/E_L$. (\hbar is set to be unity).

Expanding the fermion and dimer field operators in terms of the Bloch wave functions $\phi_{nk}(x)$ and $\Phi_{NK}(x)$, with $n, N = \{0, 1, 2, \dots\}$ the band index and $k, K \in (-k_L, k_L]$ the crystal momentum, the Hamiltonian (1) can be written as:

$$\mathcal{H} = \sum_{nk} \epsilon_{nk} \psi_{nk}^\dagger \psi_{nk} + \sum_{NK} (E_{NK} + \nu) d_{NK}^\dagger d_{NK} + \frac{g}{\sqrt{L}} \sum_{NK} \sum_{nn'; kk'} \left(c_{nn'; kk'}^{NK} d_{NK}^\dagger \psi_{nk} \psi_{n'k'} + h.c. \right) \quad (2)$$

where ϵ_{nk} and E_{NK} are respectively the eigen-energies of fermion and dimer Bloch states, and $c_{nn';kk'}^{NK}$ is the atom-dimer coupling constant. One can check that a non-zero $c_{nn';kk'}^{NK}$ requires $k + k'$ identical to K up to an integer reciprocal vector. Therefore K is a good number during the scattering process.

We write down the two-body ansatz with a fixed K :

$$|\Psi\rangle = \sum_{nn'} \sum_{k>K/2} \alpha_{nn';k} \psi_{nk}^\dagger \psi_{n',K-k}^\dagger + \sum_N \beta_N d_{NK}^\dagger \quad (3)$$

By imposing the Schrödinger equation $\mathcal{H}|\Psi\rangle = E|\Psi\rangle$, we can obtain a coupled set of equations for $\{\alpha_{nn';k}\}$ and $\{\beta_N\}$, which can be further reduced to

$$\left(\frac{m}{2l_o} - M_{NN}\right) \beta_N = \sum_{N' \neq N} M_{NN'} \beta_{N'} \quad (4)$$

with

$$M_{NN'} = \left(-\frac{m^2 r_o}{2}(E - E_{NK}) + \frac{1}{L} \sum_k \frac{k^2}{2\epsilon_k}\right) \delta_{NN'} + \frac{1}{L} \sum_{nn';kk'} \frac{c_{nn';kk'}^{NK} c_{nn';kk'}^{N'K}}{E - \epsilon_{nk} - \epsilon_{n',k'}}. \quad (5)$$

In writing above equations, we have utilized the renormalization equations for l_o , r_o [19, 20]. Since the lattice configuration will not affect the scattering in high-energy space, the two ultraviolet divergences in the diagonal terms of M-matrix can exactly cancel with each other.

We remark that Eq.4 is applicable to any interaction strength/range, lattice depth and total momentum K . Its left and right sides respectively describe the scattering process within each dimer level and between different levels, with the latter process caused by the coupling between relative and center-of-mass motions for two particles moving in lattices. Similar coupled equations were also developed for s-wave interacting fermions in a 3D lattice[7, 9]. In this work, we will focus on the two-body ground state with $K = 0$, and simplify $c_{nn';kk'}^{N,K=0}$ as $c_{nn';k}^N$.

Bound state spectrum. The bound state solution can be obtained by requiring nontrivial solutions of $\{\beta_N\}$ in Eq.4. In Fig.1a, we show the bound state spectrum with range $r_o = 0.5a_L$ at lattice depth $v = 6$. As increasing $1/l_o$, we can see a series of bound states emerging from the two-body continuum, corresponding to the coupled-channel ($\{N\}$) solutions in Eq.4. Given the property that $M_{NN'}$ is finite only when $N - N'$ is even, these bound states fall into two classes: one is by coupling even- N dimer levels (solid lines in Fig.1a), which produces a symmetric two-body wave-function in the center-of-mass motion: $\Psi(x_1, x_2) = \Psi(-x_2, -x_1)$; the other is by coupling odd- N (dashed lines), and produces asymmetric wave function: $\Psi(x_1, x_2) = -\Psi(-x_2, -x_1)$. We see that the ground state belongs to the symmetric class.

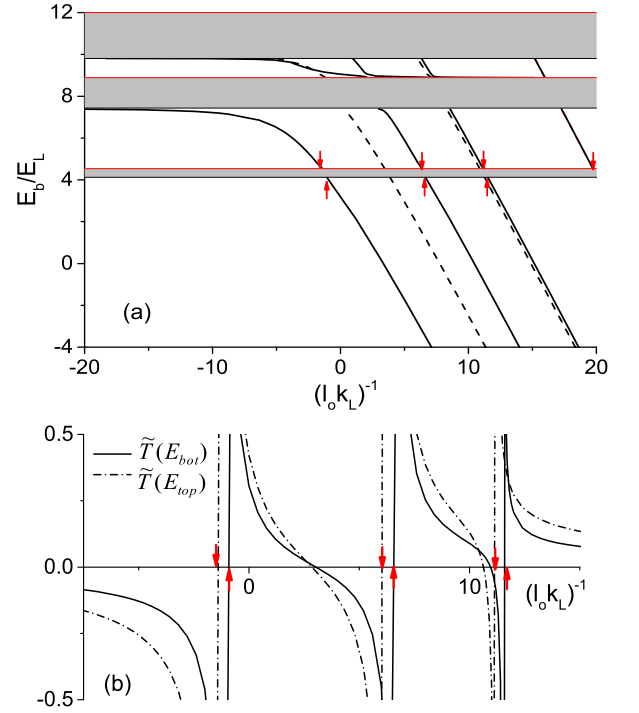


FIG. 1. (Color online). (a) Bound state energy E_b (in unit of E_L) and (b) the scaled T-matrix \tilde{T} (in unit of $(mLk_L)^{-1}$) for Bloch-wave scattering near the lowest band bottom (solid lines) and top (dashed-dot) as functions of $1/(l_o k_L)$. Here $v = 6$, $r_o = 0.5a_L$. In (a), the solid (dashed) lines correspond to symmetric (asymmetric) center-of-mass motions(see text). The upward (downward) arrows in (a,b) mark the emergence of attractive (repulsive) bound states near the lowest band, where $\tilde{T}(E_{bot})$ ($\tilde{T}(E_{top})$) go across resonances.

Bloch-wave resonance. The bound states emergent at the bottom and top of each continuum band in Fig.1a imply the scattering resonances of Bloch waves at corresponding energy. In general, for any two-body scattering state $\Psi(E) = |n, k_0; n', -k_0\rangle$ (E is the total energy), the on-shell scattering matrix $T(E)$ can be obtained by summing up all virtual scatterings to the dimer and two-fermion intermediate states[20]. The resulted $T(E)$ can be expressed[7] by introducing the eigenvector R_N^α and corresponding eigenvalue χ_α for M-matrix in Eq.(5), which gives

$$T(E) = 2 \sum_{\alpha} \frac{|\sum_N R_N^\alpha c_{nn';k_0}^N|^2}{\frac{m}{2l_o} - \chi_\alpha}. \quad (6)$$

Once $m/(2l_o)$ matches one of the eigenvalues χ_α , $T(E)$ will go through a resonance, with the width determined by the nominator of above equation.

In Fig.1b, we plot the scaled T-matrix, $\tilde{T} = T/\Delta k^2$, for Bloch states scattering near the lowest-band bottom ($\Delta k = k_0 \rightarrow 0$) and the top($\Delta k = k_L - k_0 \rightarrow 0$) at $v = 6$, respectively denoted by $\tilde{T}(E_{bot})$ and $\tilde{T}(E_{top})$. Multiple resonances are shown as tuning $1/l_o$. As only

even-N dimer levels couple with the lowest-band scattering state, these resonances are associated with the labels $\alpha = 0, 2, 4, \dots$ in Eq.(6). Combined with Fig.1a, one can see that the emergences of attractive (or repulsive) bound states correspond to the resonance of $\tilde{T}(E_{bot})$ from $-\infty$ to $+\infty$ (or $\tilde{T}(E_{top})$ from $+\infty$ to $-\infty$).

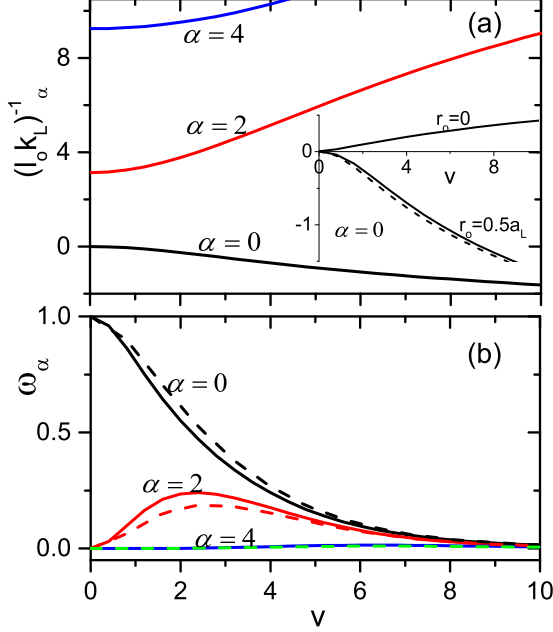


FIG. 2. (Color online). Resonance locations $(l_o k_L)^{-1}_\alpha$ (a) and widths ω_α (b) as functions of v for the first three resonances of $\tilde{T}(E_{bot})$ in Fig.1b. Inset of (a) shows the first resonance locations with zero and finite ranges, respectively; the dashed line shows the prediction to finite-range case based on the zero-range result and decoupled-channel analysis (see text). Dashed lines in (b) shows $(c_{00;k_0}^{N=\alpha}/k_0)^2$.

In Fig.2(a,b), we plot out the resonance locations $(l_o k_L)^{-1}_\alpha$ and widths $\omega_\alpha = |\sum_N R_N^\alpha c_{00;k_0}^N|^2/k_0^2$ for the first three resonances of $\tilde{T}(E_{bot})$ as changing v . We can see that as v increases from zero, the first resonance ($\alpha = 0$) moves from $1/l_o = 0$ (free-space resonance) to $1/l_o < 0$ side (weak coupling), with resonance width gradually decreases; while the rest ones ($\alpha = 2, 4$) move to $1/l_o > 0$ side (strong coupling), with widths initially increasing and finally decreasing with v . As shown below, these features manifest the unique interplay between lattices and odd-wave interactions with finite range.

First, we analyze the finite range effect to the resonance locations. For comparison, in the inset of Fig.2a we plot the first resonance locations ($\alpha = 0$) for both finite and zero r_o . One can see that as v increases, the resonance with $r_o = 0$ moves to $1/l_o > 0$ side, on contrary to the finite r_o case. A qualitative understanding can be gained from the decoupled-channel assumption, i.e., by neglecting all $M_{N \neq N'}$ in Eq.5. In this case the resonance is solely determined by matching M_{NN}

with $m/2(1/l_o + \Delta_N)$, with $\Delta_N = mr_o(E_{bot} - E_{N0})$ giving the difference of the N-th resonance locations between zero and finite r_o cases. As shown in the inset of Fig.2a, $\Delta_{N=0}(> 0)$ gives a very good approximation to such difference for the first resonance. In $v \gg 1$ limit, $(E_{bot} - E_{00})$ is roughly the zero-point energy for the relative motion of two atoms in a single well, so we expect the first resonance occur in the very weak coupling regime $1/l_o \sim -v^{1/2}r_o/a_L^2$. Note that this should be distinguished from the induced resonances in 3D with arbitrarily weak s-wave interaction[4, 6, 7], where the enhanced on-site coupling, rather than the range effect, plays a dominated role.

Secondly, the behavior of ω_α can also be qualitatively understood from the decoupled-channel analysis, where $R_N^\alpha = \delta_{N\alpha}$ and $\omega_\alpha = (c_{00;k_0}^\alpha/k_0)^2$, as shown by dashed lines in Fig.2b. A remarkable feature here is that all ω_α decay with v in $v \gg 1$ limit. Physically, this is because the odd-wave interaction uniquely favors fermion-fermion correlation between neighboring lattice sites, which can be greatly suppressed by the potential barrier of deep lattices. This is in sharp contrast to the s-wave interacting case, where one of resonance widths can be greatly enhanced by on-site correlations for large v [7]. Here due to the comparable widths for large v (see Fig.2b, $\omega_{0,2}$ are of the same order for $v \geq 4$), one has to treat multiple Bloch-wave resonances at equal footing.

Effective model. Based on the two-body solutions, we can construct an effective model, H_{eff} , for open-channel fermions in the lowest band. Given the multiple resonances that ought to be treated equally in general, we include in H_{eff} all levels of closed-channel dimers. Specifically, H_{eff} corresponds to projecting the original fermion operators in Eqs.(1,2) to the lowest band, while keeping the dimer operators with all bands involved. Accordingly, the detuning ν and coupling g are respectively replaced by the effective ones ν_{eff} and g_{eff} . These two parameters resulted in an effective interaction strength $U_{eff} = -2g_{eff}^2/\nu_{eff}$ and a finite range $r_{eff} = -(m^2 g_{eff}^2)^{-1}$. As U_{eff} and r_{eff} have encapsulated all contributions from higher-band scatterings, they can be seen as *regularized* interaction parameters for the lowest-band fermions.

We determine U_{eff} and r_{eff} by matching the T-matrix from effective model, T_{eff} , with the exact values (Eq.6) for Bloch-wave scattering at the bottom and the top of the lowest band. Specifically, T_{eff} reads

$$T_{eff}(E) = 2 \sum_\alpha \frac{|\sum_N \bar{R}_N^\alpha c_{00;k}^N|^2}{\frac{1}{U_{eff}} - \bar{\chi}_\alpha}, \quad (7)$$

where \bar{R}_N^α and $\bar{\chi}_\alpha$ are respectively the eigenvector and eigen-value of the matrix $\bar{M}(E)$ with elements:

$$\bar{M}_{NN'} = -\frac{m^2 r_{eff}}{2} (E - E_{NK}) \delta_{NN'} + \frac{1}{L} \sum_k \frac{c_{00k}^N * c_{00k}^{N'}}{E - \epsilon_{0k} - \epsilon_{0,K-k}}.$$

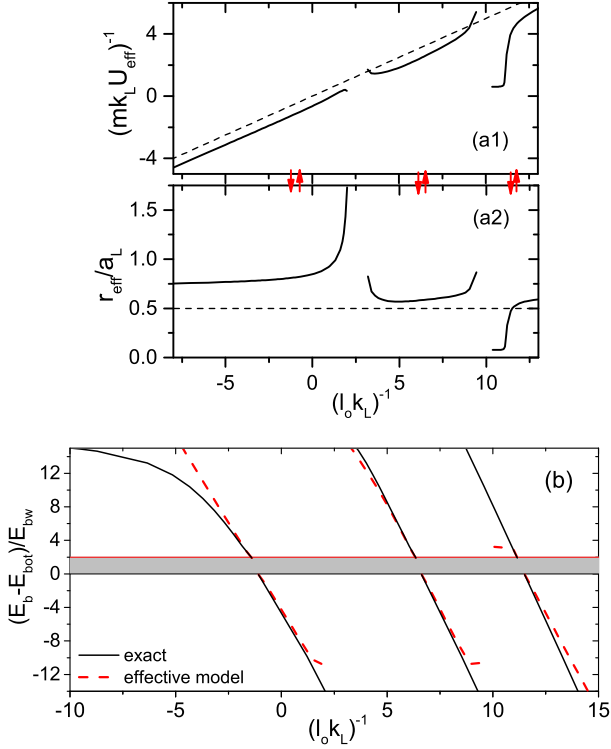


FIG. 3. (Color online). (a1,a2) Effective parameters U_{eff}^{-1} and r_{eff} near the three resonances as shown in Fig.1b. The dashed lines in (a1,a2) show the effective interaction and range for free space: $U_{\text{eff}} = 2l_o/m$ and $r_o = 0.5a_L$. The up- and down-ward arrows mark the resonance positions of $\tilde{T}(E_{\text{bot}})$ and $\tilde{T}(E_{\text{top}})$. (b) Bound state spectrum from exact solutions (black solid lines, same as Fig.1a) and from effective model (red dashed) near the lowest band. Here energies are scaled by the single-particle band width E_{bw} .

Thus Eq.7 can also predict multiple scattering resonances. Since both T (Eq.6) and T_{eff} (Eq.7) are multi-value functions of interaction parameters, to ensure a one-to-one mapping between $1/l_o$ and $1/U_{\text{eff}}$, we require the resulted T and T_{eff} are near the same order of resonance, i.e., dominated by the same dimer level. Such procedure leads to the solution of U_{eff} and r_{eff} as shown in Fig.3(a1,a2), which reproduce both $\tilde{T}(E_{\text{bot}})$ and $\tilde{T}(E_{\text{top}})$ in Fig.1b. We can see that both U_{eff} and r_{eff} differ from the free-space results $2l_o/m$ [19] and $0.5a_L$ (dashed lines in Fig.3(a1,a2)), due to the renormalized high-band contributions. We have not determined U_{eff} and r_{eff} far from resonances, as in this regime the resonance order is obscure to define.

We test the validity of H_{eff} by calculating the two-body binding energy E_b , which is determined by matching $1/U_{\text{eff}}$ with an eigen-energy of $\tilde{M}(E_b)$ -matrix (i.e., when $T_{\text{eff}} \rightarrow \infty$ in Eq.7). As shown in Fig.3b, E_b can well reproduce the exact solutions for attractive and repulsive bound states near Bloch-wave resonances, even within an energy range up to 5 – 10 times the single-

particle band width for the first two resonances. Meanwhile, we note that the effective model only works in a very narrow parameter window for the bound states near the third resonance. This can be attributed to its extremely narrow width $\omega_4 \sim 0.014 \ll \omega_{0,2}$ (see Fig.2b). Accordingly, outside the resonance regime the associated bound states have much less weight in the lowest band than the higher ones, and thus the effective model for the lowest-band fermions fails to work in that regime.

To this end, we have confirmed the validity of H_{eff} in predicting both the scattering amplitudes and the bound states above/below the lowest-band near the Bloch-wave resonances. We have checked that the single-channel model, i.e., without including closed-channel dimers[7], is unable to predict the correct bound state solutions. Our scheme here to determine the effective parameters is also different from previous ones for s-wave interacting fermions[8, 9, 21].

Finally, we convert H_{eff} to lattice model by expanding field operators in terms of Wannier functions, $\psi(x) = \sum_i \psi_i \omega_0(x - R_i)$; $d(x) = \sum_{N,i} d_{N,i} W_N(x - R_i)$, giving

$$H_{\text{eff}} = -t_f \sum_{\langle i,j \rangle} (\psi_i^\dagger \psi_j + h.c.) - \sum_{\langle i,j \rangle; N} t_d^{(N)} (d_{N,i}^\dagger d_{N,j} + h.c.) + \sum_i \epsilon_f \psi_i^\dagger \psi_i + \sum_i (\epsilon_d^{(N)} + \nu_{\text{eff}}) d_{N,i}^\dagger d_{N,i} + g_{\text{eff}} \sum_{N,i,\delta_1,\delta_2} \left(c_{\delta_1,\delta_2}^{(N)} d_{N,i+\delta_1}^\dagger \psi_i \psi_{i+\delta_2} + h.c. \right), \quad (8)$$

where t_f and ϵ_f ($t_d^{(N)}$ and $\epsilon_d^{(N)}$) are the nearest-neighbor hopping and on-site potential of fermions (dimers at level N); the coupling $c_{\delta_1,\delta_2}^{(N)} = -i \int dx W_N^*(x - \delta_1 a_L) (\omega_0'(x) \omega_0(x - \delta_2 a_L) - \omega_0(x) \omega_0'(x - \delta_2 a_L))$. Fixing $\delta_2 = 1$, we show in Fig.4a that $|c_{\delta_1,\delta_2}^{(N)}|$ is the largest when $\delta_1 = 0$ or 1. We have checked that given a general δ_2 , $|c_{\delta_1,\delta_2}^{(N)}|$ is the largest when $\delta_1 = [\delta_2/2]$ or $[(\delta_2 + 1)/2]$, i.e., when the dimer sits in the center of two fermions to optimize the atom-dimer coupling. In Fig.4b, we plot the largest $|c_{\delta_1,\delta_2}^{(N)}|$ as a function of δ_2 , and find it gradually decreases as δ_2 increases from 1. Thus to capture the most dominated atom-dimer coupling in deep lattices, we can choose the nearest-neighbor fermions $\delta_2 = 1$ and dimers sitting with either one of the fermions $\delta_1 = 0$ or 1.

Compared to the Kitaev chain model[1], this lattice Hamiltonian (Eq.8) additionally includes a multiple level of closed-channel dimers. These dimers together with the coupling to fermions play the role of neighbor-site pairing in the Kitaev model. Given the additional inner structure of dimers at different levels and the highly tunable interaction strength in (8), the Majorana fermions, if exist, are expected to show a richer property in the current system.

Summary. In summary, we have addressed the two-body effective scattering and bound states for 1D Fermi gases in optical lattices across odd-wave resonances. The

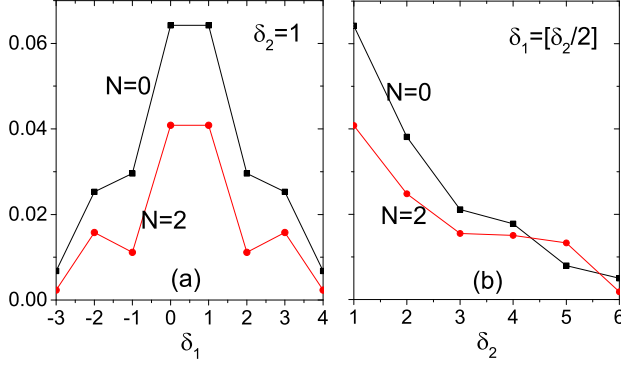


FIG. 4. (Color online). Lattice model parameter $|c_{\delta_1, \delta_2}^{(N)}|$ (in unit of $a_L^{-3/2}$) for $N = 0, 2$ at $v = 6$. In (a) $\delta_2 = 1$; in (b) $\delta_1 = [\delta_2/2]$.

multiple Bloch-wave resonances with comparable widths, the associated attractive/repulsive bound states, and the effect of finite interaction range can be detected in current cold atoms experiments. In addition, we have constructed an effective low-energy model, which successfully describes both the scattering amplitudes and bound states near the lowest band. As an analog of the Kitaev chain to host Majorana fermions[1], the effective model sets the basis for future exploring topological quantum states in realistic 1D cold atomic systems.

Acknowledgment. The work is supported by the National Natural Science Foundation of China (No.11374177, No. 11534014), the National Key Research and Development Program of China (2016YFA0300603), and the National Science Foundation under Grant No. NSF PHY11-25915. The author would like to thank the hospitality and support of the Kavli Institute for Theoretical Physics in Santa Barbara during the program "Universality in Few-Body Systems" in the winter of 2016, where this manuscript was partly

finished.

-
- [1] A.Y. Kitaev, Phys. Usp. **44**, 131 (2001).
 - [2] E. Majorana, Nuovo Cimento **5**, 171 (1937).
 - [3] F. Wilczek, Nat. Phys. **5**, 614 (2009); S. R. Elliott and M. Franz, Rev. Mod. Phys. **87**, 137 (2015).
 - [4] P. O. Fedichev, M. J. Bijlsma, and P. Zoller, Phys. Rev. Lett. **92**, 080401 (2004).
 - [5] R. B. Diener and T.-L. Ho, Phys. Rev. Lett. **96**, 010402 (2006).
 - [6] X. Cui, Y. Wang and F. Zhou, Phys. Rev. Lett. **104**, 153201 (2010).
 - [7] H. P. Buchler, Phys. Rev. Lett. **104**, 090402 (2010).
 - [8] J. von Stecher, V. Gurarie, L. Radzihovsky, and A. M. Rey, Phys. Rev. Lett. **106**, 235301 (2011).
 - [9] M. L. Wall and L. D. Carr, Phys. Rev. Lett. **109**, 055302 (2012).
 - [10] K. Winkler, G. Thalhammer, F. Lang, R. Grimm, J. H. Denschlag, A. J. Daley, A. Kantian, H. P. Buechler and P. Zoller, Nature **441**, 853 (2006).
 - [11] C. A. Regal, C. Ticknor, J. L. Bohn, and D. S. Jin, Phys. Rev. Lett. **90**, 053201 (2003).
 - [12] C. Ticknor, C. A. Regal, D. S. Jin, and J. L. Bohn, Phys. Rev. A **69**, 042712 (2004).
 - [13] J. Zhang, E. G. M. van Kempen, T. Bourdel, L. Khaykovich, J. Cubizolles, F. Chevy, M. Teichmann, L. Tarruell, S. J. J. M. F. Kokkelmans, and C. Salomon, Phys. Rev. A **70**, 030702 (R)(2004).
 - [14] C. H. Schunck, M. W. Zwierlein, C. A. Stan, S. M. F. Raupach, W. Ketterle, A. Simoni, E. Tiesinga, C. J. Williams, and P. S. Julienne, Phys. Rev. A **71**, 045601 (2005).
 - [15] K. Gunter, T. Stoferle, H. Moritz, M. Kohl, and T. Esslinger, Phys. Rev. Lett. **95**, 230401 (2005).
 - [16] B. E. Granger and D. Blume, Phys. Rev. Lett. **92**, 133202 (2004).
 - [17] L. Pricoupenko, Phys. Rev. Lett. **100**, 170404 (2008).
 - [18] S.-G. Peng, S. Tan, and K. Jiang, Phys. Rev. Lett. **112**, 250401 (2014).
 - [19] X. Cui, Phys. Rev. A **94**, 043636 (2016).
 - [20] X. Cui and H. Dong, arxiv:1608.00183 (to appear in Phys. Rev. A).
 - [21] L. M. Duan, Phys. Rev. Lett. **95**, 243202 (2005).